Open Fault Detection in Variable Phase-Pole Machines Based on Harmonic Plane Decomposition

Yixuan Wu, *Graduate Student Member, IEEE*, Gustaf Falk Olson, *Graduate Student Member, IEEE*, Claes Henriksson, and Luca Peretti, *Senior Member, IEEE*

***Abstract*—Multiphase electrical machine are inherently fault tolerant due to the higher number of phases. An important step in achieving a fault tolerant control is the ability to detect and identify the fault. In variable phase-pole drives, which are a class of multiphase machines that change the number of pole pairs during real-time operation, there are further unexplored possibilities. Based on the harmonic plane decomposition theory for variable phase-pole machine, a fault detection and identification algorithm is proposed, which analyzes the spatial harmonics of the current distribution. The fault detection is fast, operation independent, noninvasive, parameter-insensitive, and computationally simple. Experimental tests validate the proposed method.**

***Index Terms*—Discrete Fourier transform, fault detection, harmonic plane decomposition, multiphase electric machines, variable phase-pole machine.**

NOMENCLATURE

Variables

m	Number of phases.
p	Number of pole pairs.
$Q_{[.]}$	Number of slots.
γ	Spatial phase shift between magnetic axes.
δ	Dirac delta function.
$\mathbf{x}_{[.]}$	Real-valued vector of $x_{[.]}$
h	Harmonic plane.
$x_{[.]}$	Generic signal that may be replaced by a state or input variable.
t	Time.
$\bar{X}_{[.]}$	Complex notation of space vector $\mathbf{x}_{[.]}$
n_{mw}	Number of minimum windings.
K_{mw}	Factor for machine coil or toroidal coil.
ϑ	Angle of space-vector quantity.
$\omega_{[.]}$	Rotational frequency.
v_{dc}	Pole-to-pole dc-bus voltage.
$f_{[.]}$	electric frequency.
$v_{[.]}, i_{[.]}$	Time-domain voltage/current.
τ_{shaft}	Shaft torque.
k, l	Running number.
r_{th}	Amplitude threshold.
$t_{\mathrm{on}}, t_{\mathrm{off}}$	ON and OFF thresholds of time hysteresis.
h_{detect}	Harmonic plane for detecting existence of fault.
$\mathbf{h}_0$	Set of harmonic plane for localizing the fault.
$\mathbf{k}_{\mathrm{detect}}$	Set of identified faulty minimum winding indices.
k_{detect}	Identified faulty minimum winding index.
k_{f}	Faulty minimum winding.
$T_{[.]}$	Time period.
t_{detect}	Detection time: from fault impact to detection.
t_{locked}	Locking time: from fault occurrence to turn-ON of post-fault controller (PFC).
t_{fault}	Time instant of fault impact.
q	Counter for number of consecutive faulty PWM periods.
R_s, L_M, L_σ, R_R	Electrical machine parameters in the inverse Γ model.
$e_k, R_k, F_{\mathrm{th}}, F_{[.]}$	Parameters of fault detection methods in literature.
$C_{[.]}$	Clarke transformation matrix.

Subscripts

x^f	Faulty.
x^h	Healthy.
x_h	Harmonic plane.
x_r	Rotor.
x_s	Stator.
x_{123}	123 fundamental reference frame.
$x_{\alpha\beta 0}$	Stationary $\alpha\beta 0$ reference frame.
x_{dq0}	Rotary $dq0$ reference frame.

Manuscript received 3 June 2023; revised 21 November 2023; accepted 21 December 2023. Date of publication 1 January 2024; date of current version 16 February 2024. Recommended for publication by Associate Editor D. G. Xu. *(Corresponding author: Yixuan Wu.)*

The authors are with the Division of Electric Power and Energy Systems, KTH Royal Institute of Technology, 10044 Stockholm, Sweden (e-mail: yixuanw@kth.se; gufo@kth.se; claeshen@kth.se; lucap@kth.se).

Color versions of one or more figures in this article are available at https://doi.org/10.1109/TPEL.2023.3348973.

Digital Object Identifier 10.1109/TPEL.2023.3348973

I. INTRODUCTION

MULTIPHASE electrical machines (MPEMs) are becoming more and more important in the industrial and scientific world because of their high reliability, current sharing capability between inverter legs, low torque ripple, and potentially high power density as compared to the prevailing three-phase machines [1], [2], [3], [4]. Variable phase-pole machines (VPPs) additionally offer the capability to change the pole-pair number by means of control without any physical hardware reconfiguration [5], [6], [7], [8], [9], [10], [11]. Performing pole-phase modulation (PPM) [10] extends the torque-speed characteristics of VPPs, such that the applications requiring high torque at low

speed and high speed with low torque become potential applications. Electric traction applications are potential use cases for VPPs as described in [6] and [7]. Compared over the entire drive cycle, IMs can match or even outperform the energy efficiency of synchronous machines with surface magnets (PMSMs) [12]. This is mainly due to the higher efficiency in the field-weakening region, corresponding to highway driving. The same holds for multiphase IMs [13]. VPPs must, however, be carefully designed, especially concerning the stator winding structure in relation to the desired phase-pole configuration (PPC). For example, the machine designs in [5], [6], and [7] increase the degrees of freedom to a maximum by allowing for individually controllable currents in each stator slot. This design allows a plethora of PPCs. However, the benefits of pole changing are already achieved with a lower number of phases. The presented VPPs in [8] and [11] have nine phases and allow two PPCs: $[m = 3, p = 6]$ and $[m = 9, p = 2]$. Raj et al. [14] presented, based on the drive cycle of a heavy-duty electric vehicle, a similar design with two PPCs, $[m = 3, p = 3]$ and $[m = 9, p = 1]$, and showed the potential increase in power density as compared to a conventional three-phase machine. Although it is possible to create a VPP with six phases, it is not recommended due to high lateral forces on the bearings during the pole transition in a change from odd to even number of pole pairs as illustrated in [10].

Wu et al. [15] introduced the harmonic plane decomposition (HPD) as a modeling approach for VPPs and demonstrated its virtue to perform a seamless phase-pole transition. Since the HPD theory is built upon the winding structure of the machine independently from the number of phases and poles currently in operation, it appears also as a suitable candidate for fault detection in VPPs.

There has been a long tradition of considering faults in electric drives. Already in the last century, Hanna and Prabhu [16] reported that users identify semiconductor converters contribute to a large degree to a faulty drive. Although the technology has come a long way and the failure rates are sinking, semiconductor power devices are still responsible for 31% of drive failures according to surveyed users [17]. As MPEMs have an increased amount of terminal connections and power electronic switches, open-phase faults (OPFs) are more likely in MPEM drives. On the contrary, short-circuit faults have their origin in failures in the winding insulation. These are not necessarily different in an MPEM as compared to a three-phase machine, i.e., the existing approaches for conventional drives apply. Therefore, this article focuses on OPFs.

As a subgroup of MPEMs, VPPs offer the capability for true fault tolerance, i.e., post fault operation with continuous torque without increased ripple as compared to the healthy state. This is a direct consequence of the increased amount of phases where even a fault does not prevent creating a constant rotating magneto-motive force (MMF). The first step on the way to achieve true fault tolerance is the detection and localization of the fault. Recent review papers [18] and [19] summarized all the approaches made for MPEMs on the field of fault tolerance, with the focus on OPFs in [18]. Although intended for fixed-pole MPEMs, some methods are highlighted below.

According to [18], [20], [21], and [22], fault-detection algorithms should hold the following conditions:

R1) have a short detection time (shorter than one fundamental period), which is critical for post-fault control;
R2) be independent from operational conditions;
R3) be independent from machine parameters;
R4) be noninvasive, without requirements of extra hardware;
R5) avoid complex implementation.

The authors in [23] and [24] presented the phase-current-based fault detection (PHCFD) for conventional three-phase machines, and Duran et al. [20] showed its adaptation to a six-phase machine, however, argued that PHCFD has the following significant disadvantages.

1) The fault indicators e_k are nonzero for a healthy phase during faulty operation.
2) A high precision estimation of the fundamental period T_s is necessary, otherwise the fault indicator e_k is nonzero in healthy operation.
3) A moving average is needed, i.e., the lower boundary for the detection time is one fundamental period T_s.

In order to mitigate the aforementioned shortcomings, the authors in [20] and [21] proposed the vector-space-decomposition fault detection (VSDFD). It leverages the increased number of phases by detecting the fault in the xy vector-space. With the assumption of a perfectly sinusoidally distributed stator winding, the components in the xy vector space should always be zero as they do not contribute to the torque production [20]. However, this is not the case of generic MPEMs and VPPs, where all harmonics up to the number of phases can produce torque with the exception of zero sequences [25]. The authors of [21] and [22], as an extension of [20], made the same assumption for a five-phase machine with distributed windings. In the Clarke transformation, the xy vector-space resembles the harmonic plane $h = 2$ in the HPD theory. The simplicity of the fault indicators R_k is a consequence of the fact that there are only two harmonic planes in both machines. It is notable that the authors in [21] and [22] pointed out that the fault indicators R_k differ with the machine configuration, i.e., PPC. In fact, the fault indicators also depend on the choice of the Clarke transformation matrix. Therefore, this method is less suitable for VPPs, as fault indicators for each PPC are necessary.

Other strategies for detecting an OPF based on the analysis of the stator currents were presented in [26] and [27]. Despite being developed for PMSMs, the same analysis holds for the stator windings of an induction machine-based VPP. Applying the superposition approach of a set on faulty currents with the healthy set of currents models the faulty behavior of the machine. Analyzing the harmonic faulty currents in the xy vector-space identifies a distinct direction for each single faulty switch. The directions depend on the number of phases, the order of the harmonic plane, and the location of the fault.

First, Wang et al. [26] detected the existence of a fault by observing the amplitude of the current space-vector in the xy harmonic plane, which corresponds to $h = 5$ in the HPD theory. If the amplitude exceeds the threshold of 1 A, the existence of a fault is detected. Next, the average of all possible

predefined axes is computed over one fundamental period T_s with the axis with the smallest component to be perpendicular to the faulty winding. This sets the fault detection time to exactly T_s which the authors show in their experimental results.

Trabelsi et al. [27] dealt with a PMSM with potentially nonsinusoidal back-electromotive force and also disregarded the assumption of sinusoidal stator windings, it cannot be generally assumed that $\bar{I}_{xy}$ is zero. The proposed centroid-based fault detection and isolation (CBFDI) computes the average location of a centroid spanned by the current space-vector $\bar{I}_{xy}$ with the α-axis. The resulting minimum detection time takes at least about one fundamental period T_s, contrasting with requirement $R1$.

A recent article [28] proposed a method to observe the oscillation of the fundamental current space vector with respect to the output angular position of a PLL. The oscillation originates from the compensation actions of the controller based on a so-called magnetic field pendulous oscillation (MFPO). This approach requires as well one fundamental period for the detection of a fault.

All the abovementioned fault detection strategies have in common that they are intended for fixed-pole MPEMs. The number of phases have a maximum of six. Consequently, there is one unexcited harmonic plane, often called the xy plane, next to a homopolar axis or plane. This limits the fault detection time to one fundamental period T_s, as only after one period the direction of the faulty current space-vector can be identified with certainty. In contrast, reasonable VPP designs have at least nine phases, and thus, at least four harmonic planes. Moreover, these IM-based VPPs always have a magnetizing current, facilitating current-based fault detection methods.

This article proposes a fault detection method based on the HPD, taking advantage of the increased amount of harmonic planes and, thus, filling the gap in fault detection for VPPs. According to the authors' best knowledge, there exist no literature targeting VPPs specifically. It modifies the superposition approach from [26] and [27], by leveraging the HPD theory. Instead of observing the current space vector over time, the harmonic-plane-decomposition fault detection (HPDFD) uses the spatial current distribution. This shortens the fault detection time to lower than one fundamental period by omitting the computation of the centroid or the average value. It fulfills all the abovementioned requirements ($R1 - R5$) and is generally valid for any PPC of a VPP.

The HPD theory from [15] provides the healthy machine model for this work. Section II derives the impact of a fault from the inverse Clarke transformation. Further, it describes the model based on a superposition of healthy and faulty currents. Section III describes the detection of an open fault in two steps: 1) existence of the fault and 2) its location. Experimental results in Section IV show a loaded OPF and open-switch fault (OSF) with the proposed fault detection in place. In addition, comparative results show the shortened fault detection time due to the shift from time to spatial information. Finally, Section V concludes this article.

The proposed fault-detection algorithm can be applied in combination with the fault-tolerant controller in [29] minimizing the stator copper losses. This work is a continuation of the conference proceedings [30] with experimental data.

II. Open-Switch/Phase Fault in Harmonic Plane Decomposition

This section describes the constraints introduced by an OSF or OPF to the machine model using the HPD theory.

A. Harmonic Plane Decomposition

The basis for the here proposed fault detection algorithm has its foundations in the HPD theory [15]. The theory creates a unified model for all possible PPCs in a VPP by analyzing the spatial harmonics of a space-vector quantity. For the work in this article, the stator currents are analyzed in the stationary $\alpha\beta 0$ reference frame. The stator side transformation matrix in (1) transforms the measured currents in 123 reference frame [31] to the $\alpha\beta 0$ reference frame

$$\mathbf{x}_{\alpha\beta 0} = \underbrace{\left(\frac{2}{n_{\mathrm{mw}}}\right)^{K}}_{\mathbf{T}_{123\to\alpha\beta 0}} \mathbf{C}_s \cdot \mathbf{x}_{123} \quad \mathbf{x}_{123} = \underbrace{\left(\frac{2}{n_{\mathrm{mw}}}\right)^{1-K}}_{\mathbf{T}_{\alpha\beta 0\to 123}} \mathbf{C}_s^{\mathrm{T}} \cdot \mathbf{x}_{\alpha\beta 0}$$

$$\mathbf{C}_s = \begin{bmatrix} 1 & \cos(1\gamma) & \cos(2\gamma) & \dots & \cos((n_{\mathrm{mw}}-1)\gamma) \\ 0 & \sin(1\gamma) & \sin(2\gamma) & \dots & \sin((n_{\mathrm{mw}}-1)\gamma) \\ 1 & \cos(2\gamma) & \cos(4\gamma) & \dots & \cos((n_{\mathrm{mw}}-1)2\gamma) \\ 0 & \sin(2\gamma) & \sin(4\gamma) & \dots & \sin((n_{\mathrm{mw}}-1)2\gamma) \\ \vdots & \vdots & \vdots & \ddots & \vdots \\ 1 & \cos\left(\frac{n_{\mathrm{mw}}}{2}\gamma\right) & \cos\left(2\frac{n_{\mathrm{mw}}}{2}\gamma\right) & \dots & \cos\left((n_{\mathrm{mw}}-1)\frac{n_{\mathrm{mw}}}{2}\gamma\right) \\ 0 & \sin\left(\frac{n_{\mathrm{mw}}}{2}\gamma\right) & \sin\left(2\frac{n_{\mathrm{mw}}}{2}\gamma\right) & \dots & \sin\left((n_{\mathrm{mw}}-1)\frac{n_{\mathrm{mw}}}{2}\gamma\right) \end{bmatrix}.$$

$$\gamma = \frac{\pi}{K_{\mathrm{mw}} n_{\mathrm{mw}}} \tag{1}$$

B. Open-Switch/Phase Impact

This work considers the following types of open faults:

F1) OPF—no current in faulty winding k_{f};
F2) upper OSF—no positive current in faulty winding k_{f};
F3) lower OSF—no negative current in faulty winding k_{f}.

Fault F1) typically appears when the windings are damaged, the terminal connection is lost or the driving circuit fails. F1) can also be a combination of the faults F2) and F3).

In case of F2) and F3), the upper or lower switch malfunctions. The cause may be a semiconductor failure, affecting both switch and diode in antiparallel. Another reason is a fault in the driver circuit, preventing the switches to turn on. However, in both cases, the winding cannot be connected to the dc+ (F2) or dc− (F3) leading to a lack of positive (F2) or negative (F3) current.

Despite having different origins, the consequences of all faults F1), F2), and F3) are similar. In the faulty steady state, F1) prevents any current flow, whereas, F2) prevents positive and F3) prevents negative current flow in the faulty minimum winding.

In case of an open fault, the system describing the VPP reduces in rank. As an example, (2) shows the additional constraint introduced by a fault in minimum winding $k_{\mathrm{f}} = 1$. This can

be derived by examining the inverse Clarke transformation in (1) as follows:

$$i_{s,1} = 0 = \sum_{h=1}^{\frac{n_{\mathrm{mw}}}{2}} i_{\alpha,h}. \tag{2}$$

The formerly decoupled harmonic planes become, therefore, coupled; in this case, the α-components sum to zero.

C. Superposition of Healthy and Faulty Current

As Trabelsi et al. [27] already suggested, the currents after the occurrence of an OSF or OPF can be divided into two parts in the fundamental 123 reference frame: 1) a healthy set of currents $\mathbf{i}^h_{s,123}$ and 2) a faulty set of currents $\mathbf{i}^f_{s,123}$

$$\begin{aligned}\mathbf{i}_{s,123} &= \mathbf{i}^h_{s,123} + \mathbf{i}^f_{s,123}\\ \mathbf{i}^f_{s,123} &= [i^f_{s,1}, i^f_{s,2}, \dots i^f_{s,n_{\mathrm{mw}}}]^{\mathrm{T}}.\end{aligned} \tag{3}$$

By separating the healthy from the faulty part, the detection relies on the analysis of the faulty space-vector currents $\mathbf{i}^f_{s,123}$. Considering a fault in a single minimum winding k_{f}, the faulty set currents are as follows:

$$i^f_{s,k} = \begin{cases} -i^h_{s,k} & \text{if} \quad k = k_{\mathrm{f}} \quad \text{F1,F2: } i^h_{s,k} > 0 \quad \text{F1,F3: } i^h_{s,k} < 0 \\ 0 & \text{else.} \end{cases} \tag{4}$$

For each time instance, this is in fact a Dirac δ-function shifted by k_{f} with varying amplitude

$$i^f_{s,k} = -i^h_{s,k}\delta\left(k - k_{\mathrm{f}}\right).$$

As the generalized Clarke transformation from (1) performs a discrete Fourier transformation (DFT) as explained in [15], the faulty current space-vectors in each harmonic plane $\bar{I}^f_{\alpha\beta0,h,k_{\mathrm{f}}}$ is described by

$$\begin{aligned}\bar{I}^f_{\alpha\beta0,h,k_{\mathrm{f}}} &= \sum_{k=1}^{n_{\mathrm{mw}}} -i^h_{s,k}\delta\left(k - k_{\mathrm{f}}\right) e^{j\frac{2\pi}{n_{\mathrm{mw}}}(k-1)h}\\ &= -i^h_{s,k_{\mathrm{f}}} e^{j\frac{2\pi}{n_{\mathrm{mw}}}(k_{\mathrm{f}}-1)h} = i^f_{s,k_{\mathrm{f}}} e^{j\frac{2\pi}{n_{\mathrm{mw}}}(k_{\mathrm{f}}-1)h}\\ &= \left[\cos\left(\vartheta_{h,k_{\mathrm{f}}}\right) + j\sin\left(\vartheta_{h,k_{\mathrm{f}}}\right)\right] i^f_{s,k_{\mathrm{f}}}\\ \vartheta_{h,k_{\mathrm{f}}} &= h\gamma(k_{\mathrm{f}} - 1)\\ \gamma &= \frac{2\pi}{n_{\mathrm{mw}}}.\end{aligned} \tag{5}$$

It can be seen that the current space-vector $\bar{I}^f_{\alpha\beta0,h,k_{\mathrm{f}}}$ corresponds to the projection of the current $i^f_{s,k_{\mathrm{f}}}$ on the harmonic plane h with the phase angle $\vartheta_{h,k_{\mathrm{f}}}$, which is a function of the harmonic plane order h and the position of the minimum winding k_{f} where the fault occurred. Fig. 1 visualizes this relation (5) in one harmonic plane in the $\alpha\beta0$ reference frame.

The above analysis is a generalization of the reference directions in [26] and [27]. Applying $\gamma = 72^\circ$ for the symmetrical five-phase machine and analyzing the harmonic plane $h = 3$ according to the HPD theory yields exactly the same result as in [27]. Similarly, applying $\gamma = 30^\circ$ and examining $h = 5$ yields the same result as in [26], once the windings are transformed into the 123 fundamental reference frame. The presented strategy recognizes the existence of further harmonic planes, which improves the detection speed and robustness in the same time.

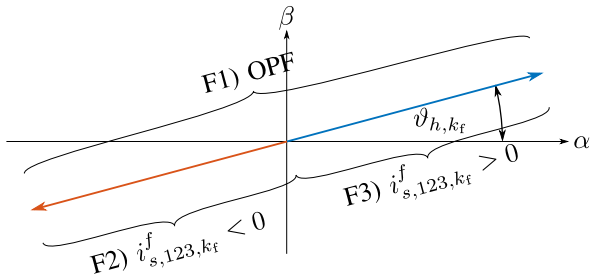

Fig. 1. Directions of faulty current space-vector $\bar{I}^f_{\alpha\beta0,h,k_{\mathrm{f}}}$ in harmonic plane h for a faulty minimum winding k_{f}. The polarity of $i^f_{s,123,k_{\mathrm{f}}}$ determines the direction of $\bar{I}^f_{\alpha\beta0,h,k_{\mathrm{f}}}$.

III. Fault Identification Process

This section elaborates on the HPDFD. It examines the superpositioned fault current $i^f_{s,123,k_{\mathrm{f}}}$ in the $\alpha\beta0$ reference frame using the HPD theory. The proposed HPDFD is divided into the following two steps.

1) Detection of the Existence of an Open-Switch/Phase Fault: The first step is to identify the existence of a fault. Any fault is recognized as an imbalance in the spatial current distribution, which is, therefore, analyzed.

The HPD theory is exclusively based on the defined minimum windings n_{mw} of the stator in order to unify all possible PPCs. In fact, one PPC does not excite all harmonic planes h during healthy operation, i.e., some harmonic planes remain with zero currents. It is highlighted that the unexcited harmonic planes depend on the chosen PPC. Hence, choosing one of these harmonic planes for detection, called h_{detect}, and observing the current space-vector's amplitude $|\bar{I}|_{\alpha\beta0,h_{\mathrm{detect}}}$ may detect the existence of an significant imbalance, e.g. a potential fault.

In reality, all machines inherently have some imbalance, in addition to omnipresent measurement noise. Consequently, the amplitude of the current space-vectors in the harmonic plane h_{detect} deviate from zero even in healthy state. To account for these factors, an amplitude threshold r_{th} along with a time hysteresis $[t_{\mathrm{on}}, t_{\mathrm{off}}]$ are set for the detection. Fig. 2 shows the schematic for the complete algorithm to detect the existence of a fault in each PWM period. A counter q increases in case the current space-vector $|\bar{I}|_{\alpha\beta0,h_{\mathrm{detect}}}$ in h_{detect} exceeds the threshold r_{th} (6). When the counter reaches $\frac{t_{\mathrm{on}}}{T_{\mathrm{sw}}}$, the state is set to *faulty* and the counter is limited, which is equal to the fault being present for at least t_{on}. In case $|\bar{I}|_{\alpha\beta0,h_{\mathrm{detect}}}$ falls below r_{th}, the counter q decreases until it reduces under a value $\frac{t_{\mathrm{off}}}{T_{\mathrm{sw}}}$ and the state is set to *healthy*. Together a time hysteresis is reached for the detection of the existence of a fault

$$|\bar{I}|_{\alpha\beta0,h_{\mathrm{detect}}} > r_{\mathrm{th}}. \tag{6}$$

Choosing the homopolar in the machine of interest as h_{detect} has the benefit that in healthy control, the current space-vector

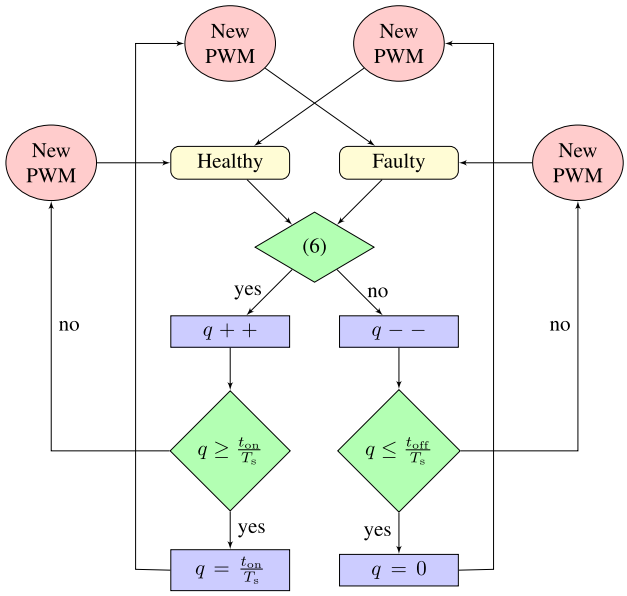

Fig. 2. Algorithm for detection of the existence of a fault with amplitude threshold and time hysteresis in each PWM period.

is close to zero. The choice of the hysteresis time thresholds, t_{on} and t_{off}, poses a tradeoff between robustness and detection time.

2) Detection of the Fault Location: Knowing the existence of a fault, it is possible to determine its location. Utilizing the dependency of ϑ_{h,k_f} in (5), the instantaneous angle of $\bar{I}_{\alpha\beta0,h,k_\text{f}}$ reveals the faulty winding, if h is not excited.

However, measurement noise, as well as the impact of the healthy current controller, may displace $\bar{I}_{\alpha\beta0,h,k_\text{f}}$ from its ideal direction. In order to be certain about the fault location, previously presented fault detection strategies without the assumption of sinusoidal winding distribution observed the angle of $\bar{I}_{\alpha\beta0,h,k_\text{f}}$ over one fundamental period. Leveraging on the virtue of VPPs that they have at least four harmonic planes, the proposed HPDFD achieves a shorter fault detection time by extracting the spatial current distribution over a set of unexcited harmonic planes $\mathbf{h}_0$. In this work, the average of the instantaneous relative angles between the harmonic planes $\mathbf{h}_0$ are used. Consequently, the more harmonic planes $\mathbf{h}_0$ contains, the more reliable the detection becomes. If one chooses to use fewer harmonic planes for fault localization, it is advised to use low order harmonic planes since the spatial angle resolution is higher, i.e., one electrical degree corresponds to fewer mechanical degrees.

Equation (7) shows the angle differences between harmonic planes within the set $\mathbf{h}_0$. The resulting vector of angle differences $\Delta\boldsymbol{\vartheta}_{k_\text{f}}(l)$, therefore, contains one entry less than $\mathbf{h}_0$

$$\Delta\boldsymbol{\vartheta}_{k_\text{f}}(l) = \angle\left(\underline{I}^{f}_{\alpha\beta0,\mathbf{h}_0(l+1),k_\text{f}}\right) - \angle\left(\underline{I}^{f}_{\alpha\beta0,\mathbf{h}_0(l),k_\text{f}}\right)$$
$$l \in [1, |\mathbf{h}_0| - 1]\,. \tag{7}$$

Further, (8) normalizes the angle differences $\Delta\boldsymbol{\vartheta}_k$ with the minimum winding pitch angle γ and the set of harmonic orders $\mathbf{h}_0$ yielding the inversion of the expression for ϑ_{h,k_f} in (5)

$$k_{\text{detect,j}} = \left\lfloor \frac{\sum \frac{\Delta\boldsymbol{\vartheta}_{k_\text{f}}(l)}{(\mathbf{h}_0(l+1)-\mathbf{h}_0(l))\gamma}}{|\mathbf{h}_0| - 1} \right\rceil + 1. \tag{8}$$

It is noted that (8) rounds the index to the nearest integer number as the computation may result in noninteger results. Moreover, $k_{\text{detect,j}}$ is the computed location in the jth PWM period.

In a final step, choosing the most recurring value of k_{detect} as in (9) over all previous PWM periods increases the reliability of the localization of the fault.

$$k_{\text{detect}} = \text{mode}\left(k_{\text{detect,j}}, k_{\text{detect,j}-1}, k_{\text{detect,j}-2}, \dots\right) \tag{9}$$

Consequently, the longer the detection is allowed to settle, the more reliable the HPDFD becomes. This poses another tradeoff between fault detection time and robustness. After a defined time t_{locked}, the identified faulty winding is considered sufficiently certain and the drive may switch to a PFC. It is noted that the HPDFD does not depend on any particular PFC. Once the fault is locked, the PFC remains operational until a scheduled maintenance is performed.

B. Fault Detection Time

The proposed HPDFD's detection time has a lower boundary set by the amplitude threshold r_{th}, the time hysteresis ($t_{\text{on}}/t_{\text{off}}$) from Section III-1 and the locking time t_{locked} from Section III-2. In the theoretical analysis in [30], an instantaneous fault detection was achieved due the instantaneous spatial harmonics of the current distribution. Different from [20], [21], [22], [23], [24], and [27], the underlying theoretical root of this algorithm does not require any averaging over a fundamental period T_s nor a moving average over a predefined time T_m. However, the proposed method requires at least two harmonic planes for the fault detection and a third one producing the torque. The more harmonic planes are available to the fault detection, the faster it may become.

The practical implementation of the HPDFD has a nonzero fault detection time. The addition of the time hysteresis and the majority vote improve the robustness and counteract measurement noise and inherent machine asymmetries. Thus, the tradeoff is to set these times such that the ubiquitous noise floor does not trigger false-positives and simultaneously it is acceptable for the drive to operate without proper PFC within the minimum detection time. However, this can be very application specific. The same tradeoff between detection time and robustness was reported in [20], [21], and [27].

IV. Experimental Results

In this section, the proposed algorithm detects an OPF and an OSF in a VPP with individual solenoidal windings in each stator slot. The drive uses the controllers described in [15] and the PFC from [29] with minimum stator copper losses.

Fig. 3 depicts the experimental setup, and Fig. 4 schematically depicts the terminal connections. In addition, a circuit breaker (blue) or an IGBT switch (pink) is inserted between the converter

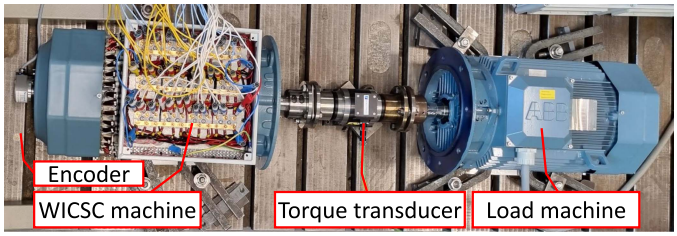

Fig. 3. Solenoidal winding VPP with load machine.

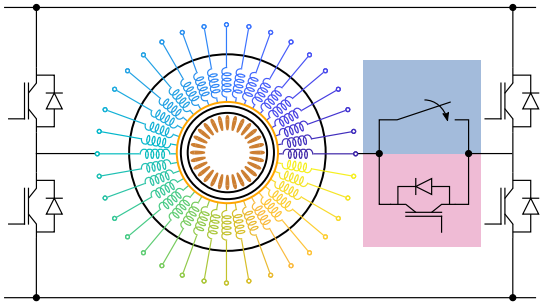

Fig. 4. Schematic of the VPP with $Q_s = 36$ independent stator coils (color shade) and $Q_r = 28$ rotor bars (brown). For an OPF, a breaker imitates the fault (blue area). For an OSF, an IGBT switch turns OFF to prevent current flow in one direction (pink area). Only two inverter legs are shown for clarity.

TABLE I
ELECTRICAL PARAMETERS OF THE VPP

h	R_s	L_σ	L_M	R_R	h	R_s	L_σ	L_M	R_R
1	318	5.6	155	203	10	318	3.5	3.2	53
2	318	4.5	38.2	126	11	318	3.5	3.2	53
3	318	4.2	16.5	101	12	318	3.5	3.2	53
4	318	3.9	8.7	82	13	318	3.5	3.2	53
5	318	3.8	5.4	68	14	318	3.5	3.2	53
6	318	3.5	3.2	53	15	318	6.7	-	-
7	318	3.5	3.2	53	16	318	6.3	-	-
8	318	3.5	3.2	53	17	318	6.0	-	-
9	318	3.5	3.2	53	18	318	5.5	-	-

Resistances in [mΩ] and inductances in [mH].

output and the winding k_f to emulate an OPF or an OSF, respectively. At time instance $t_\mathrm{fault} = 0$ s, the circuit breaker or the IGBT switch is opened emulating a fault. The direction of the IGBT determines whether an upper or lower OSF is emulated. Using an IGBT has the advantage that the shut-off behavior of a real semiconductor switch is emulated in the experiment.

A. Real Time Implementation

For a first experiment, the proposed HPDFD is implemented for real time operation on the drive, which runs in the $[m = 18, p = 1]$ PPC. Table I lists the electrical parameters of the tested VPP. The VPP runs in cascaded speed and current control at $\omega_r = 1001$ r/min. The load machine is set such that $\tau_\mathrm{shaft} = 10\,\mathrm{Nm}$ is maintained. The dc-bus voltage is $v_\mathrm{dc} = 107\,\mathrm{V}$. An OPF and a lower OSF are introduced to the faulty winding $k_\mathrm{f} = 10$. Table II summarizes the tuning parameters for the presented experiments in the HPDFD. For the detection of the existence of an OPF/OSF, the homopolar component $h_\mathrm{detect} = 18$ is chosen. For the localization of the fault, the harmonic planes $\mathbf{h}_0 = [7, \ldots, 17]$ are chosen. In this VPP, the harmonic planes $h \leq 6$ can be excited in order to achieve PPCs with at least three phases. Fig. 5 shows the time domain currents $\{i_9, i_{10}, i_{11}\}$ along with ω_r and τ_shaft. In the figure, the following four time instances are marked.

TABLE II
FAULT IDENTIFICATION TUNING PARAMETERS

h_detect	r_{th}	$t_\mathrm{ON}/t_\mathrm{OFF}$	t_locked	$\mathbf{h}_0$
18	$0.15 \cdot \hat{i}_{123}$	$0.1 \cdot \frac{2\pi}{\omega_s}$ / $0.9 t_\mathrm{on}$	$0.2 \cdot \frac{2\pi}{\omega_s}$	$[7, \ldots, 17]$

1) **Breaker:** The breaker is being opened. The current waveform becomes distorted but remains nonzero. In case of the OPF, the contact must disengage entirely, the contact resistance must rise and any potential arc has to decay. In case of the OSF, the IGBT has to fully discharge and block the current flow.
2) **Fault:** The current in the faulty slot becomes zero.
3) **Detect:** The fault detection algorithm identifies the correct slot as faulty.
4) **Locked:** The fault detection algorithm locks the faulty slot and turns on the PFC.

In addition, the fault detection time t_detect, defined as the time between **Fault** and **Detect**, and the total time before the PFC t_locked, defined as the time between **Breaker** and **Locked**, are given in milliseconds as well as fraction of the fundamental period are given in the figure.

The fault detection time $t_\mathrm{detect} = 13.4\,\mathrm{ms}$ in Fig. 5(a) is significantly shorter than one fundamental period with 22.3%. The fault detection time $t_\mathrm{detect} = 49.3\,\mathrm{ms}$ in Fig. 5(b) is closer to one fundamental period with 82.1%. However, as the current goes through one positive half-wave, where no fault is detected since the fault has no impact on the current, the effective time in which the fault has an impact is much lower. Removing the time of the positive half-period, the detection time shrinks to 32.1%. The total reaction time for the OPF is $t_\mathrm{locked} = 41.6\,\mathrm{ms}$ corresponding to 69.4% of the fundamental period. In case of the OSF, it is $t_\mathrm{locked} = 65.9\,\mathrm{ms}$ corresponding to 109.8% of the fundamental period; again there is a healthy half period included in this number.

In both cases, at time instance **Breaker**, the torque drops leading to a dip in the speed. The healthy controller counteracts the loss of one winding by increasing the current amplitude in the other remaining windings. In contrast, the PFC maintains the τ_shaft and, thus, ω_r with a smaller current peak than the healthy controller. Tani et al. [29] explained the details of this PFC.

For a more detailed presentation, Figs. 6 and 8 show the normalized average current space vectors $\bar{I}_{\alpha\beta 0,h,k}$ for the harmonic planes $\mathbf{h}_0$ between **Fault** and **Locked** for an OPF and OSF, respectively. Furthermore, the angles in $\Delta\boldsymbol{\vartheta}_{h,k_\mathrm{f}}$ are marked with their index l. According to the theory in (5), the expected angles are $\vartheta_{\mathbf{h}_0,k_\mathrm{f}=10} = [\frac{3}{2}\pi, 0, \frac{1}{2}\pi, \pi, \ldots]$. However, it can be observed that the current space-vectors are rotated toward the expected direction. Nevertheless, the angle differences are sufficiently close to the expected $\frac{1}{2}\pi$. Figs. 7 and 9 show the identified faulty

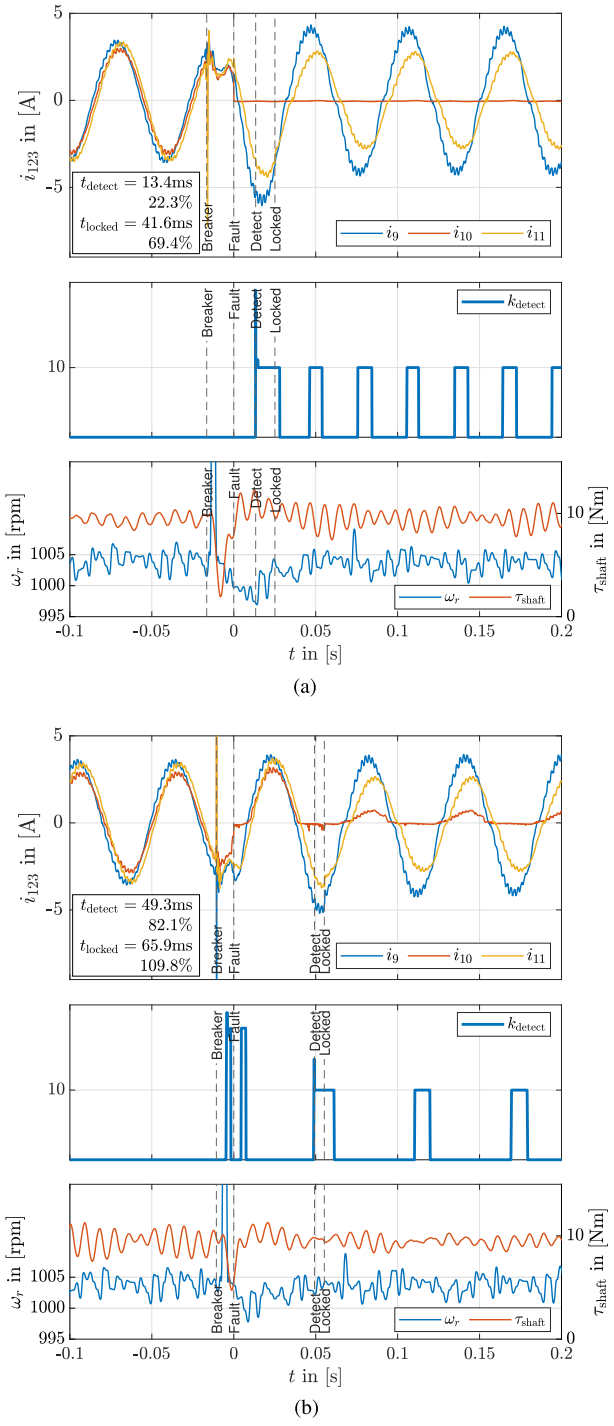

Fig. 5. Slot currents $i_{(9,10,11)}$ for a faulty slot $k_{\text{f}} = 10$. (a) Open-phase fault (OPF). (b) Lower open-switch fault (OSF).

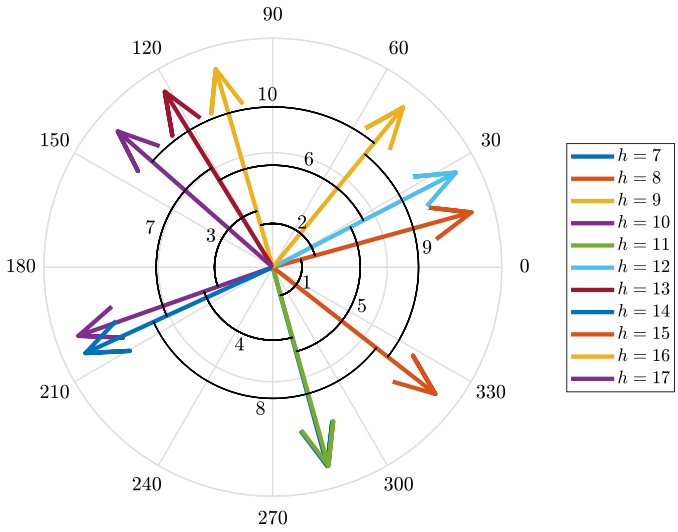

Fig. 6. Normalized average space vectors $\bar{I}_{\alpha\beta 0,h,k}$ for harmonic planes in $\mathbf{h}_0$ in the OPF.

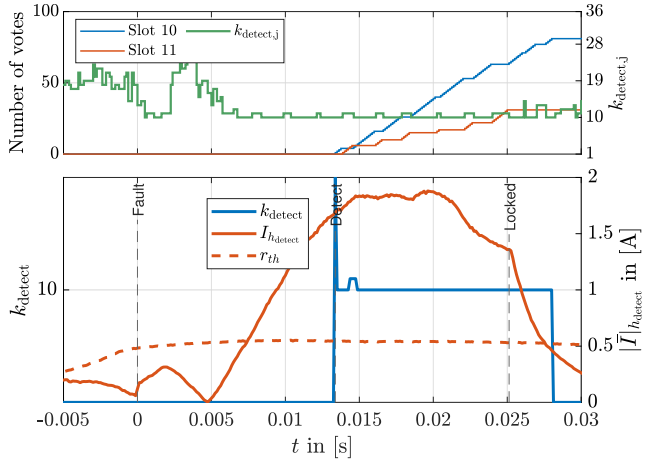

Fig. 7. OPF in $k_{\text{f}} = 10$: Identified faulty minimum winding $k_{\text{detect,j}}$ in each PWM period and the evolution of majority vote over time for the two most votes minimum windings. Amplitude of current space vector $|\bar{I}|_{\alpha\beta 0,h_{\text{detect}}}$, amplitude threshold r_{th}, identified faulty minimum winding after majority vote k_{detect}.

minimum winding in each PWM period $k_{\text{detect,j}}$ following (8) for an OPF and OSF, respectively. Further, the evolution of cumulated votes for the two most identified minimum windings before the majority vote are plotted. In addition, they show the amplitude of current space vector $|\bar{I}|_{\alpha\beta 0,h_{\text{detect}}}$, amplitude threshold r_{th}, and the identified faulty minimum winding after majority vote k_{detect} according to (9). The delay in fault detection from $|\bar{I}|_{\alpha\beta 0,h_{\text{detect}}}$ exceeding the threshold r_{th} are visible for both type of faults. From $k_{\text{detect,j}}$ in Fig. 7, it is notable that the proposed HPDFD outputs the neighboring minimum winding for some time instances, which can be explained by the current space-vectors in $\mathbf{h}_0$ being rotated in comparison to the ideal directions as depicted in Fig. 6. However, the correct minimum winding is identified significantly more often and the majority vote over time solves this issue and assures that the correct faulty minimum winding is determined.

In case of the OSF, Fig. 9 shows that the HPDFD identifies the existence of a fault before **Fault** because the current imbalance is already significantly large. However, $k_{\text{detect,j}}$ does not correspond to the actual faulty winding unless the current in k_{f} reaches zero. This emphasizes the importance of introducing t_{locked}. It is emphasized that the current waveform between **Breaker** and **Fault** may differ significantly depending on the root cause of the fault. Nevertheless, the proposed algorithm

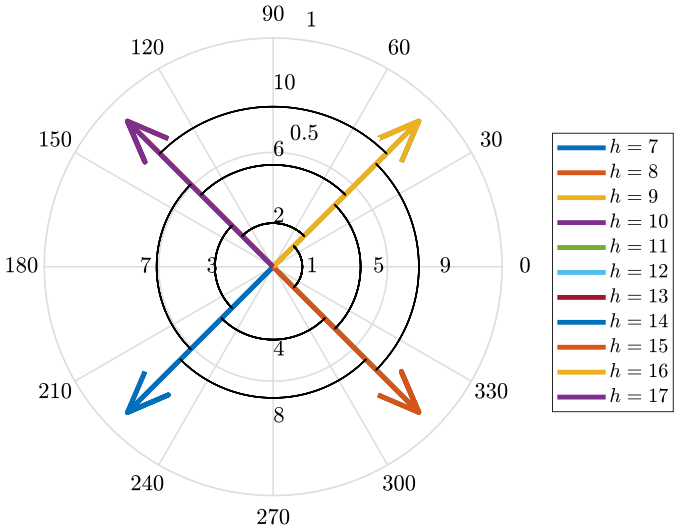

Fig. 8. Normalized average space-vectors $\bar{I}_{\alpha\beta 0,h,k}$ for harmonic planes in $\mathbf{h}_0$ in the OSF.

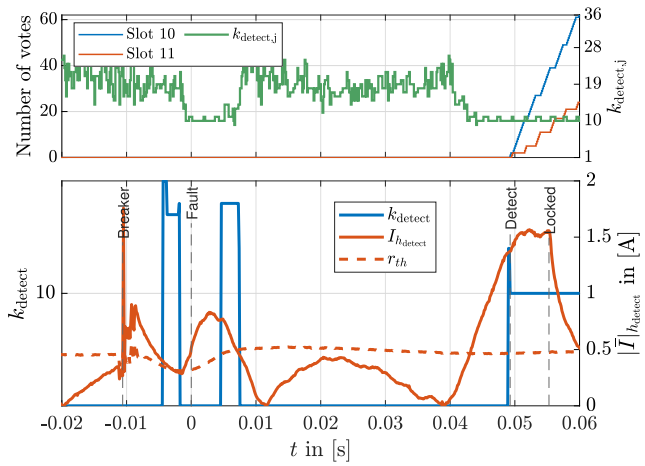

Fig. 9. Lower OSF in $k_{\text{f}} = 10$: Identified faulty minimum winding $k_{\text{detect,j}}$ in each PWM period and the evolution of majority vote over time for the two most votes minimum windings. Amplitude of current space-vector $|\bar{I}|_{\alpha\beta 0,h_{\text{detect}}}$, amplitude threshold r_{th}, identified faulty minimum winding after majority vote k_{detect}.

is independent of the root cause as it analyzes the current imbalance.

B. Comparative Experiments

In the second set of experiments, the drive is configured in an 18-phase full bridge configuration and operated in $[m = 18, p = 1]$ PPC. The drive operates at $\omega_r = 1000$ r/min at $\tau_{\text{shaft}} = 10$ Nm, while at $t_{\text{fault}} = 0$ s the breaker is operated for an OPF in $k_{\text{f}} = 10$. For the sake of comparison, the drive continues to operate with the healthy current controllers. In postprocessing, the proposed HPDFD and the CBFDI [27] are implemented for the recorded currents. The CBFDI is chosen as it does not assume sinusoidal winding distribution, which is a key factor for VPPs.

TABLE III
FAULT IDENTIFICATION TUNING PARAMETERS FOR HPDFD AND CBFDI

h_{detect}	r_{th}	$\mathbf{h}_0$	F_{th}
17	$0.05 \cdot \hat{i}_{123}$	$[3, 5, 7 \ldots, 17]$	0.05

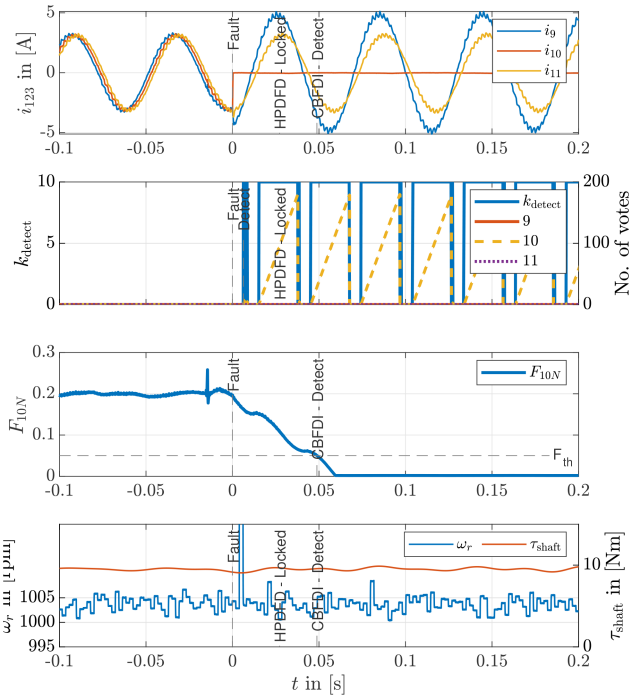

Fig. 10. Comparative results for an OPF in $k_{\text{f}} = 10$ for HPDFD and CBFDI. The VPP drive is in an 18-phase full bridge configuration and runs in $[m = 18, p = 1]$ PPC.

Table III shows the tuning parameters for the HPDFD, which differ from the previous experiment. Due to the full bridge configuration, only odd harmonic planes are available, leading to the different choices for h_{detect} and $\mathbf{h}_0$. Further, the current controllers are tuned more aggressively for this hardware configuration, which leads to the decrease of r_{th}. Moreover, F_{th} has been lowered as the steady state value is lower than in [27]. Fig. 10 juxtaposes the results for both fault detection methods. For the HPDFD, $k_{\text{detect,j}}$ is shown along with the received votes of the faulty and its neighboring healthy windings. For the CBFDI, the indicator for a fault in $k_{\text{f}} = 10$, $F_{10\text{N}}$ is plotted. In a direct comparison, it shows that the HPDFD shortens the fault detection time by 0.0216 s or 79.6% in this experiment. The reason to this reduction is the shift from current waveform information over time to spatial current distribution information along the stator.

C. Computation Time

Finally, the computational burden is measured. The test bench uses a *Xilinx Zynq-7000 SoC ZC706 Evaluation Kit* [32] for the computation. ADC measurement deserialization, clocking, and modulation are implemented in the FPGA and the CPU executes the calculations for the closed loop control. The PWM period

in the presented setup is 125 μs. The average execution time in the CPU is 89.043 μs. The average computation time for the proposed HPDFD is 0.4631 μs, corresponding to 0.5201% of the closed loop execution time and 0.3705% of the PWM period. With the abovementioned computation time, requirement (R5) is considered to be fulfilled.

V. Conclusion

This work presents a fault detection algorithm based on the HPD theory for OPFs as well as OSFs, using information from multiple harmonic planes that are not used for torque generation. The algorithm analyzes the spatial harmonics of the stator currents in $\alpha\beta 0$ reference frame. In experiments, the proposed algorithm shows that its detection time is shorter than one fundamental period ($R1$). Furthermore, the exploitation of stator current harmonics is always feasible in any operation condition ($R2$) and independent of machine parameters ($R3$). The proposed algorithm only requires current measurements, i.e., not requiring more hardware than the one used for closed-loop control ($R4$). Computationally, it requires one trigonometric operation next to basic mathematics per harmonic plane ($R5$). Thus, it fulfills all the requirements ($R1$–$R5$) for an open-fault detection algorithm.

The proposed method requires at least two unexcited harmonic planes for fault detection and one harmonic plane for torque production. Since existing VPP designs have at least nine phases, the proposed HPDFD is applicable to all of these VPPs.

References

[1] E. Levi, R. Bojoi, F. Profumo, H. A. Toliyat, and S. Williamson, "Multiphase induction motor drives - a technology status review," *IET Electric Power Appl.*, vol. 1, no. 4, pp. 489–516, 2007.

[2] E. Levi, "Advances in converter control and innovative exploitation of additional degrees of freedom for multiphase machines," *IEEE Trans. Ind. Electron.*, vol. 63, no. 1, pp. 433–448, Jan. 2016.

[3] F. Barrero and M. J. Duran, "Recent advances in the design, modeling, and control of multiphase machines—Part I," *IEEE Trans. Ind. Electron.*, vol. 63, no. 1, pp. 449–458, Jan. 2016.

[4] M. J. Duran and F. Barrero, "Recent advances in the design, modeling, and control of multiphase machines—Part II," *IEEE Trans. Ind. Electron.*, vol. 63, no. 1, pp. 459–468, Jan. 2016.

[5] K. Bitsi, O. Wallmark, and S. Bosga, "An induction machine with wound independently-controlled stator coils," in *Proc. 22nd Int. Conf. Elect. Machines Syst.*, 2019, pp. 1–5.

[6] G. Dajaku and D. Gerling, "Low costs and high efficiency asynchronous machine with stator cage winding," in *Proc. IEEE Int. Electric Veh. Conf.*, 2014, pp. 1–6.

[7] E. Libbos, B. Ku, S. Agrawal, S. Tungare, A. Banerjee, and P. T. Krein, "Loss minimization and maximum torque per ampere operation for variable-pole induction machines," *IEEE Trans. Transport. Electrific.*, vol. 6, no. 3, pp. 1051–1064, Sep. 2020.

[8] B. Ge, D. Sun, W. Wu, and F. Z. Peng, "Winding design, modeling, and control for pole-phase modulation induction motors," *IEEE Trans. Magn.*, vol. 49, no. 2, pp. 898–911, Feb. 2013.

[9] M. P. Magill and P. T. Krein, "A dynamic pole-phase modulation induction machine model," in *Proc. IEEE Int. Electric Machines Drives Conf.*, 2015, pp. 13–19.

[10] M. Osama and T. A. Lipo, "Modeling and analysis of a wide-speed-range induction motor drive based on electronic pole changing," *IEEE Trans. Ind. Appl.*, vol. 33, no. 5, pp. 1177–1184, Sep./Oct. 1997.

[11] B. P. Reddy, A. Iqbal, S. Rehaman, M. Meraj, and S. Keerthipati, "Dynamic modelling and control of pole-phase modulation based multiphase induction motor drives," *IEEE Trans. Emerg. Sel. Topics Power Electron.*, vol. 10, no. 3, pp. 3383–3394, Jun. 2022.

[12] V. T. Buyukdegirmenci, A. M. Bazzi, and P. T. Krein, "Evaluation of induction and permanent-magnet synchronous machines using drive-cycle energy and loss minimization in traction applications," *IEEE Trans. Ind. Appl.*, vol. 50, no. 1, pp. 395–403, Jan./Feb. 2014. [Online]. Available: https://ieeexplore.ieee.org/document/6524023

[13] Y. Matsuyama, K. Ishizuka, T. Kosaka, H. Matsumori, and N. Matsui, "Design study on high torque density multiphase pole-change induction motor for vehicle propulsion drive," in *Proc. 24th Int. Conf. Elect. Machines Syst.*, 2021, pp. 426–431. [Online]. Available: https://ieeexplore.ieee.org/document/9634455

[14] R. Raj, P. Subramaniyane, and L. Peretti, "Design of a variable phase-pole induction machine for electric vehicle applications," in *Proc. Int. Conf. Elect. Machines*, 2022, pp. 976–982. [Online]. Available: https://ieeexplore.ieee.org/document/9910688

[15] Y. Wu, G. F. Olson, and L. Peretti, "Pole-transition control of variable-pole machines using harmonic-plane decomposition," *IEEE Trans. Ind. Electron.*, vol. 70, no. 8, pp. 7753–7760, Aug. 2023.

[16] R. A. Hanna and S. Prabhu, "Medium-voltage adjustable-speed drives-users' and manufacturers' experiences," *IEEE Trans. Ind. Appl.*, vol. 33, no. 6, pp. 1407–1415, Nov./Dec. 1997.

[17] S. Yang, A. Bryant, P. Mawby, D. Xiang, L. Ran, and P. Tavner, "An industry-based survey of reliability in power electronic converters," *IEEE Trans. Ind. Appl.*, vol. 47, no. 3, pp. 1441–1451, May/Jun. 2011.

[18] A. G. Yepes, I. Gonzalez-Prieto, O. Lopez, M. J. Duran, and J. Doval-Gandoy, "A comprehensive survey on fault tolerance in multiphase ac drives, Part 2: Phase and switch open-circuit faults," *Machines*, vol. 10, 2022, Art. no. 221. [Online]. Available: https://www.mdpi.com/2075-1702/10/3/221

[19] A. G. Yepes, O. Lopez, I. Gonzalez-Prieto, M. J. Duran, and J. Doval-Gandoy, "A comprehensive survey on fault tolerance in multiphase ac drives, Part 1: General overview considering multiple fault types," *Machines*, vol. 10, 2022, Art. no. 208.

[20] M. J. Duran, I. Gonzalez-Prieto, N. Rios-Garcia, and F. Barrero, "A simple, fast, and robust open-phase fault detection technique for six-phase induction motor drives," *IEEE Trans. Power Electron.*, vol. 33, no. 1, pp. 547–557, Jan. 2018.

[21] I. González-Prieto, M. J. Duran, N. Rios-Garcia, F. Barrero, and C. Martín, "Open-switch fault detection in five-phase induction motor drives using model predictive control," *IEEE Trans. Ind. Electron.*, vol. 65, no. 4, pp. 3045–3055, Apr. 2018.

[22] P. Salas-Biedma, I. Gonzalez-Prieto, and M. J. Duran, "Current imbalance detection method based on vector space decomposition approach for five-phase induction motor drives," in *Proc. - 45th Annu. Conf. IEEE Ind. Electron. Soc.*, 2019, pp. 975–980.

[23] J. O. Estima and A. J. M. Cardoso, "A new approach for real-time multiple open-circuit fault diagnosis in voltage-source inverters," *IEEE Trans. Ind. Appl.*, vol. 47, no. 6, pp. 2487–2494, Nov./Dec. 2011.

[24] N. M. A. Freire, J. O. Estima, and A. J. M. Cardoso, "Open-circuit fault diagnosis in PMSG drives for wind turbine applications," *IEEE Trans. Ind. Electron.*, vol. 60, no. 9, pp. 3957–3967, Sep. 2013.

[25] K. Wang, Z. Y. Gu, Z. Q. Zhu, and Z. Z. Wu, "Optimum injected harmonics into magnet shape in multiphase surface-mounted PM machine for maximum output torque," *IEEE Trans. Ind. Electron.*, vol. 64, no. 6, pp. 4434–4443, Jun. 2017.

[26] X. Wang, Z. Wang, Z. Xu, M. Cheng, W. Wang, and Y. Hu, "Comprehensive diagnosis and tolerance strategies for electrical faults and sensor faults in dual three-phase PMSM drives," *IEEE Trans. Power Electron.*, vol. 34, no. 7, pp. 6669–6684, Jul. 2019.

[27] M. Trabelsi, N. K. Nguyen, and E. Semail, "Real-time switches fault diagnosis based on typical operating characteristics of five-phase permanent-magnetic synchronous machines," *IEEE Trans. Ind. Electron.*, vol. 63, no. 8, pp. 4683–4694, Aug. 2016.

[28] H. Chen, J. He, N. A. O. Demerdash, X. Guan, and C. H. T. Lee, "Diagnosis of open-phase faults for a five-phase PMSM fed by a closed-loop vector-controlled drive based on magnetic field pendulous oscillation technique," *IEEE Trans. Ind. Electron.*, vol. 68, no. 7, pp. 5582–5593, Jul. 2021.

[29] A. Tani, M. Mengoni, L. Zarri, G. Serra, and D. Casadei, "Control of multiphase induction motors with an odd number of phases under open-circuit phase faults," *IEEE Trans. Power Electron.*, vol. 27, no. 2, pp. 565–577, Feb. 2012.

[30] Y. Wu, G. F. Olson, and L. Peretti, "Fault detection in variable phase-pole machines based on harmonic plane decomposition," in *Proc. 48th Annu. Conf. IEEE Ind. Electron. Soc.*, 2022, pp. 1–6.

[31] A. A. Rockhill and T. A. Lipo, "A generalized transformation methodology for polyphase electric machines and networks," in *Proc. IEEE Int. Electric Machines Drives Conf.*, 2015, pp. 27–34.
[32] Advanced Micro Devices, Inc., "Xilinx Zynq-7000 SoC ZC706 evaluation kit," 2022. [Online]. Available: https://www.xilinx.com/products/boards-and-kits/ek-z7-zc706-g.html

Yixuan Wu (Graduate Student Member, IEEE) received the M.Sc. degree in electrical engineering, in 2019, from the RWTH Aachen University, Aachen, Germany and KTH Royal Institute of Technology, Stockholm, Sweden, where he is currently working toward the Ph.D. degree in fault tolerance in multiphase electrical machines with the Division of Electrical Power and Energy Systems (EPE).

His research interests include modeling and control of variable phase-pole drives, power electronics, fault-tolerance, and electromobility.

Gustaf Falk Olson (Graduate Student Member, IEEE) was born in Kristinehamn, Sweden. He received the M.Sc. degree in electrical power engineering, in 2016, from the KTH Royal Institute of Technology, Stockholm, Sweden, where he is currently working toward the Ph.D. degree in parameter estimation of multiphase electrical machines with the Division of Electrical Power and Energy Systems (EPE).

His research interests include modeling, control, and parameter estimation of multiphase machines for vehicle and power generation applications.

Claes Henriksson was born in Skövde, Sweden. He received the M.Sc. degree in energy and environmental technology from the KTH Royal Institute of Technology, Stockholm, Sweden, in 2022.

He is currently a Trainee with NKT HV solutions, Karlskrona, Sweden. His current research interests include control and design of electric machines, modeling of power grids, and electric heavy-duty vehicles.

Luca Peretti (Senior Member, IEEE) received the M.Sc. degree in electronic engineering from the University of Udine, Udine, Italy, in 2005, and the Ph.D. degree in electrical drives for application in mechatronics from the University of Padova, Padua, Italy, in 2009.

He is currently an Associate Professor with the Division of Electric Power and Energy Systems, KTH Royal Institute of Technology, Stockholm, Sweden, in the field of Electric Machines and Drives. Between 2007 and 2008, he was a Visiting Ph.D. Student with ABB Corporate Research, Västerås, Sweden. From 2010 to 2018, he was a Principal Scientist, Project Leader, and Strategy Coordinator with ABB Corporate Research. Since 2016, he has also been an Affiliated Faculty Member with the Division of Electric Power and Energy Systems, KTH Royal Institute of Technology. His main scientific interests include the automatic parameter estimation in electric machines, sensorless control, loss segregation in drive systems, multiphase drives, and condition monitoring of machines and drives, in the context of industrial, wind energy, and traction applications.